Optical properties and indirect-to-direct transition of GaP/AlP (001) superlattices

Masami Kumagai and Toshihide Takagahara

Nippon Telegraph and Telephone Electrical Communications Laboratories, 3-9-11 Midoricho, Musashino-shi, Tokyo 180, Japan

Eiichi Hanamura

Department of Applied Physics, The University of Tokyo, 7-3-1 Hongo, Bunkyo-ku, Tokyo 113, Japan

(Received 2 June 1987)

The electronic structure and optical properties of GaP/AlP superlattices are investigated theoretically to clarify the general features of the zone-folding and the band-mixing effects in the superlattice composed of indirect-band-gap semiconductors. The degeneracy of the minimum energies of the conduction band at the X points in the zinc-blende-type bulk materials cannot be lifted by the zone-folding effect alone. The band-mixing effect through the interfaces between two constituent materials plays an important role in determining the overall band lineup throughout the entire Brillouin zone. Thus the electronic structure of the superlattice over the entire Brillouin zone is calculated for the first time in order to determine whether the superlattice is an indirect- or direct-band-gap material. In these calculations, the sp^3s^* tight-binding method is employed which is known to yield a sufficiently accurate conduction band and to give its minimum position correctly. The electronic structure of the superlattice turns out to be quite sensitive to the combination of the well and barrier layer thickness. This sensitivity suggests the possibility of designing suitable band structures for device application. Oscillator strength in the superlattice is also estimated and is found to be larger for shorter-period superlattices in general. Because the value of the band discontinuity is quite uncertain at present, three previously reported values are applied in the calculations. The electronic structure and the optical properties are revealed for the first time to be very sensitive to the band discontinuity. To explore the possibility of designing the band structure further, the effect of applying pressure is also investigated. Applied pressure induces the changes in the electron transfer-matrix elements primarily through changes of interatomic distances and consequently modifies the electronic band structure. It is found that by applying pressure parallel to the superlattice layer, a transition can be induced from an indirect-band-gap to direct-band-gap material and thus the optical activity is enhanced. These properties suggest that the superlattice composed of indirect-band-gap semiconductors offers great potential for application to optical devices.

I. INTRODUCTION

Recently, the electronic structure of GaAs/AlAs (GaAs/Al$_x$Ga$_{1-x}$As) superlattices having direct-band-gap well layers has been investigated intensively, and the transition from a direct-band-gap material to an indirect-band-gap material (direct-to-indirect transition) has been found when the unit period of the superlattice is reduced.[1-5] However, the electronic structure of these direct-band-gap superlattices has been found to differ only slightly from that of the mixed crystal composed of the same constituent materials. In contrast to these superlattices, those which have indirect-band-gap materials as well layers can be expected to show very different properties from those of the constituent materials or their mixed crystals. This is due to the zone-folding effect which arises from the synthetic structure and the band-mixing effect through the interfaces between the constituent materials. These effects can induce a transition from an indirect-band-gap material to a direct-band-gap material (indirect-to-direct transition). Due to the k-selection rule, an interband optical transition is generally not allowed in indirect-band-gap materi-

als without the assistance of phonon scattering or impurity scattering. In the superlattice, the required k vector is supplied from the superlattice structure itself due to the zone-folding effect, and the optical transition becomes allowed without the assistance of phonon scattering.

Gnutzmann and Clausecker[6] reported the first investigation of the possibility of optical transition in structured materials consisting of indirect-band-gap materials. In their work, however, the actual energy gap of the material, which plays a significant role in optical device applications, was not estimated. Furthermore, the electrostatic potential for electrons arising from the superlattice structure was not given explicitly, although this is necessary to estimate the probability of optical transitions quantitatively. Recently, Kim and Madhukar[7] examined the electronic structure of GaP/AlP superlattices which consisted of indirect-band-gap materials in both the well and barrier layers. Their analysis of the electronic structure was limited to the Γ-Z direction and to the J points in the Brillouin zone. However, as will be shown later, it is crucially important to examine the band structure over the entire Brillouin zone in determining whether

the superlattice is a direct- or indirect-band-gap materi-al. In zinc-blende-type bulk materials, the conduction band has six equivalent minima at the X points in the x y, and z directions. The zone-folding effect in the super-lattice growth direction (z direction) brings the X_z points (X points in the z direction) to the Γ point but leaves the X_x and X_y points unchanged in the case of appropriate layer-thickness combinations. Thus when the zone-folding effect alone is taken into account, the conduction band of the superlattice has five degenerate minima: one at the Γ point and the others at the M points. The band-mixing effect through the interface of two constitu-ent materials lifts the degeneracy between these points. Thus the problem of determining the position of the conduction-band minimum is quite delicate and requires highly accurate calculation. Kim and Madhukar[7] em-ployed the conventional sp^3 tight-binding method in-cluding the second-nearest-neighbor interactions. This method is well known as a simple and convenient way of obtaining an approximate band structure and has been used successfully for calculating the structure of the valence band. However, it is well recognized that the method does not yield a reliable conduction-band struc-ture. Thus in order to determine whether the superlat-tice is a direct- or an indirect-band-gap material, we em-ployed the sp^3s^* tight-binding method[8] which is capable of yielding a more-accurate conduction-band structure. The most remarkable advantage of this method is the feasibility of band-structure calculation for large period superlattices which would make it possible to determine rather easily the layer-number combinations of the con-stituent materials which yield a direct optical transition. On the other hand, in an usual *ab initio* calculation, this determination requires a formidable amount of computa-tion time and is actually impracticable. Therefore, the tight-binding method is very quick and efficient way to survey the general features in both qualitative and quan-titative senses.

Furthermore, Kim and Madhukar's analysis was re-stricted to superlattices in which the well and barrier layers were of the same thickness. However, in our pre-liminary study,[9] the band structure of the GaP/AlP su-perlattice has been found to be very sensitive to the com-bination of the well and barrier layer thicknesses. Therefore, this paper attempts to clarify the applicability of the superlattices to optical devices by presenting a more thorough study of the optical properties as well as electronic structure of the GaP/AlP superlattice. Com-binations of the well and barrier layer thicknesses which yield direct optical transitions are also determined. Based on these results, the feasibility of designing the band structure in superlattices composed of indirect-band-gap semiconductors is discussed, and the significant potential of this synthetic material for appli-cation to optical devices is suggested for the first time.

The value of the band discontinuity between GaP and AlP is quite uncertain at present. We calculate the elec-tronic structure and optical properties of the superlattice using three previously reported values and revealed for the first time the effect of the band discontinuity on these properties. In order to further explore the possi-bility of designing the band structure, the effect of apply-ing pressure on the optical properties and electronic structure is also investigated. The application of pres-sure induces the changes in the electron transfer-matrix elements primarily through changes in interatomic dis-tances, and consequently modifies the electronic band structure. It is found that by applying pressure parallel to the superlattice layer, a transition can be induced from an indirect-band-gap material to a direct-band-gap material thus enhancing the optical activity. The band-gap energy is very sensitive to the applied pressure, and the pressure is very useful in designing the band struc-ture.

The paper is organized as follows. In Sec. II the elec-tronic structure of the GaP/AlP superlattice is present-ed. In Sec. III the optical properties of the superlattice are discussed, and the oscillator strength of the optical transition at the folded Γ point is calculated. In Sec. IV the features of the indirect-to-direct transition are clarified with respect to the combination of the well and barrier layer thicknesses. In Sec. V the effect of pressure on the GaP/AlP superlattice is presented, and the features of the indirect-to-direct transition are investigat-ed precisely. Three cases are considered according to the direction of the applied pressure. One is hydrostatic pressure, and the others are uniaxial pressure applied perpendicular and parallel to the superlattice layer. Sec-tion VI is devoted to a summary of the results and con-clusions.

II. ELECTRONIC STRUCTURE
OF THE SUPERLATTICE

In calculating the energy band structure and electron-ic wave functions, it is necessary to choose an appropri-ate method which yields a precise conduction band, be-cause in indirect well superlattices, the features of the conduction band play a large role in determining the del-icate indirect-to-direct transition. Here, the sp^3s^* tight-binding scheme is employed. In this method, the excited s-like state s^* is added to the conventional sp^3 bases in order to yield the precise conduction band. This method was first proposed by Vogl *et al.*,[10] and was extended to include second-nearest-neighbor interactions by Newman and Dow.[11] Furthermore, the tight-binding parameters were corrected by Yamaguchi.[12] In these calculations, however, dispersionless bands appear along the direction between the X point and the W point regardless of the kind of material. In the case of a monolayer superlat-tice, for example, these bands play a crucial role in determining the electronic structure, because they are folded into the direction between the Γ point and M point. Thus, the second-nearest-neighbor interactions between two p orbitals are introduced to reproduce the reference band structure precisely. Details on the calcu-lation are given in Appendix A.

The structure of a superlattice having N_a sublayers of A-compound semiconductor and N_b sublayers of B-compound semiconductor in a unit period is shown schematically in Fig. 1 using a case of GaP/AlP super-lattice as an example. Here, N is the sum of N_a and N_b.
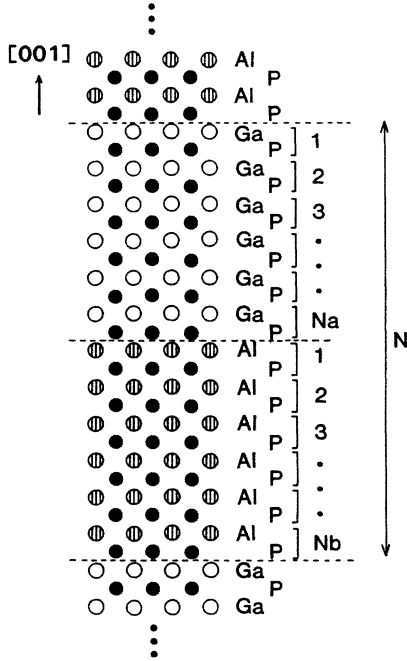
FIG. 1. Schematic diagram of the GaP/AlP superlattice.

In the following, the calculation is carried out for all combinations of N_a and N_b under the condition that $N \leq 20$. The tight-binding parameters for the bulk materials are derived from the bulk band data.[13,14] The reference values used here and the calculated values are shown in Table I. The second-nearest-neighbor interactions considered here ($U_{pp\pi}^c$ and $U_{pp\pi}^a$) are the interactions between two p_i orbitals separated by $(d/2)(\pm e_j \pm e_k)$, where i, j, and k are cyclic permutations of x, y, and z, and e_j is a unit vector in the jth direction. Here, d is the lattice constant of the material, and the suffixes c and a indicate the cation and anion, respectively. These interactions are included to reproduce the dispersion between the bulk X and W point,[15] and adjusted to yield the proper band shape. As for the X and Γ points, the energy values can be fitted exactly, whereas those at the L points cannot be fitted perfectly. The effect of the second-nearest-neighbor interactions mainly appears in the band energy near the L points, as shown in Table I. Larger values of the interactions $U_{pp\pi}^c$ and $U_{pp\pi}^a$ result in L-point energies closer to the reference values; however, they yield unpractically heavy carrier mass and unrealistic band shape.

For calculating the superlattice band structure, the first- and second-nearest-neighbor interactions between A- and B-compound semiconductors are applied here.

$U_{pp\pi}^{cc'}$ ($U_{pp\pi}^{aa'}$) stands for the second-nearest-neighbor interactions between two cations c and c' (anions a and a') lying in A- and B-compound semiconductors, respectively. In principle, these can be determined empirically by fitting the calculated band to the reference band of the superlattice. However, for the sake of simplicity, we have taken the mean value of the two bulk parameters, i.e.,

$$U_{pp\pi}^{cc'} = \tfrac{1}{2}(U_{pp\pi}^c + U_{pp\pi}^{c'}) \, ,$$

$$U_{pp\pi}^{aa'} = \tfrac{1}{2}(U_{pp\pi}^a + U_{pp\pi}^{a'}) \, . \tag{2.1}$$

With respect to the first-nearest-neighbor interaction between cations and anions lying across the interface, tight-binding parameters corresponding to C- and D-compound semiconductors are applied, which are made of cation-anion pairs c-a' and c'-a, respectively.

The GaP/AlP superlattice is chosen as the most realistic example for the investigation of the superlattice made of indirect materials. The GaP/AlP superlattice is the nearly-lattice-matched superlattice and, if necessary, a perfectly-lattice-matched superlattice can be obtained simply by using a slight amount of As-contained mixed-crystal GaAsP instead of GaP. As for the valence-band discontinuity ΔE_v of the GaP/AlP interface, a conclusive value has not been established experimentally. In this calculation, ΔE_v is treated as an unknown parameter, and the following values are employed for numerical evaluation.

Case (1): $\Delta E_0 = -0.00$ eV (Refs. 7 and 10).
Case (2): $\Delta E_v = -0.10$ eV (Refs. 7 and 10).
Case (3): $\Delta E_v = -0.46$ eV (Ref. 16).

Here, cases (1) and (2) correspond to a type-I superlattice, while case (3) corresponds to a type-II superlattice. Figure 2 shows the Brillouin zone for a monolayer superlattice ($N_a = N_b = 1$). Hereafter, the symmetry points are denoted by the same symbols as those in the figure, and the direction perpendicular to the superlattice layers is denoted by "z" and the two orthogonal directions parallel to the superlattice layers by "x" and "y". The bulk X point in the z direction is folded into the Γ point in the superlattice band, the bulk X point in the x or y direction corresponds to the M point, and the bulk L point corresponds to the R point, respectively.

The calculated band structure of the GaP/AlP monolayer superlattice is presented in Fig. 3. The superlattice bands including the second-nearest-neighbor interactions are represented by the solid curves, and the dashed curve presents the lowest conduction band neglecting the

TABLE I. Reference values and calculated values of symmetry point energies in GaP and AlP bulk crystals (in eV).

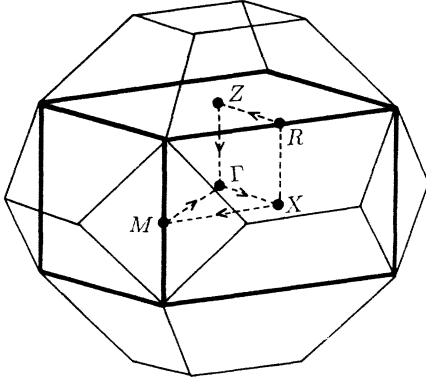|	Γ_1^v	Γ_1^c	Γ_{15}^c	X_1^v	X_3^v	X_5^v	X_1^c	X_3^c	L_1^v	L_1^c
GaP (ref.)	−13.19	2.88	5.24	−9.46	−7.07	−2.73	2.35	2.90	−1.10	2.79
GaP (calc.)	−13.19	2.88	5.24	−9.46	−7.07	−2.73	2.35	2.90	−1.21	2.61
AlP (ref.)	−12.70	3.60	5.60	−9.80	−5.40	−2.26	2.50	3.00		
AlP (calc.)	−12.70	3.60	5.60	−9.80	−5.40	−2.26	2.50	3.00	−1.08	2.95

FIG. 2. Brillouin zone for the monolayer superlattice. The Brillouin zone is also shown for zinc-blende crystal by the thin line. The familiar nomenclature of symmetry points is employed and the arrows correspond to the band structure in Fig. 3.
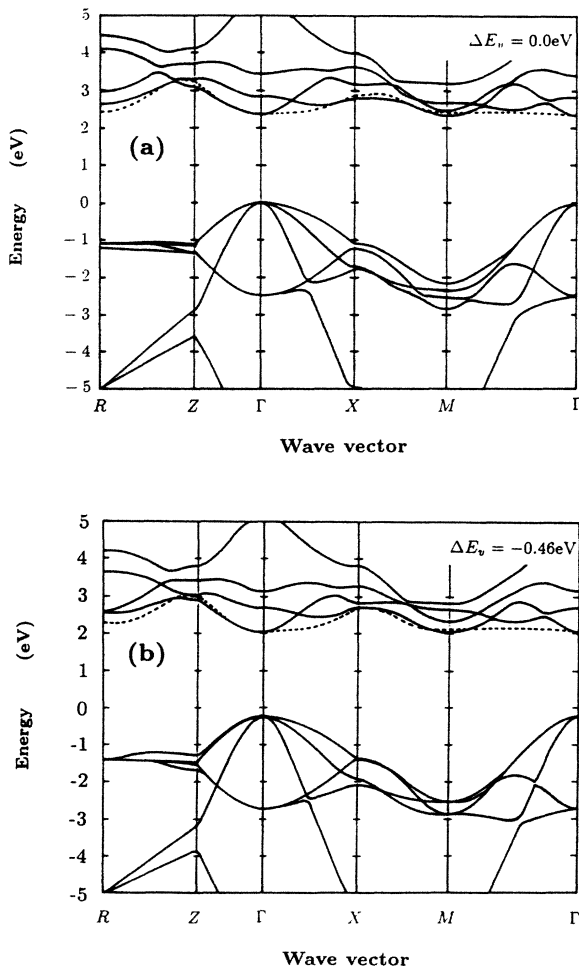
second-nearest-neighbor interactions. The results are presented for the cases of (a) $\Delta E_v = 0.00$ and (b) $\Delta E_v = -0.46$ eV. Including the second-nearest-neighbor interaction in the calculation raises the R-point energy, reflecting the fact that the interaction makes the bulk L-point energy higher. In the case of $\Delta E_v = 0.00$ eV [Fig. 3(a)], it can be seen that the superlattice is a direct-band-gap material while the original materials are both indirect-band-gap materials. A similar feature is obtained for the case of $\Delta E_v = -0.10$ eV. In the case of $\Delta E_v = -0.46$ eV [Fig. 3(b)], however, the monolayer superlattice remains an indirect-band-gap material.

These features can be explained by the zone-folding effect. Figure 4 is a conceptual diagram of this effect. In the case of $N = 2$, the Brillouin zone is reduced to half of the original Brillouin zone, and consequently the bulk X point is folded into the Γ point. The same situation holds for even numbers of N. GaP and AlP are indirect-band-gap materials having their conduction-band minimum at the X point, but the superlattice becomes a direct-band-gap material due to the zone-folding effect. It should be noted that it cannot be determined only by the zone-folding argument whether the conduction-band minimum of superlattice is at the Γ or M point, because conduction-band minima also exist at the M point which corresponds to the original bulk X points in the x and y directions.

On the other hand, the Brillouin zone for $N = 3$ is reduced to $\frac{1}{3}$ of the original Brillouin zone, and consequently the bulk X point in the z direction is not folded into the Γ point but into the z-directional edge of the Brillouin zone. The same generally holds for odd numbers of N. Therefore, the superlattice remains an indirect-band-gap material having its conduction-band minimum at the z-directional edge of the Brillouin zone. The zone-folding effect is not the only factor which causes the indirect-to-direct transition in the superlat-
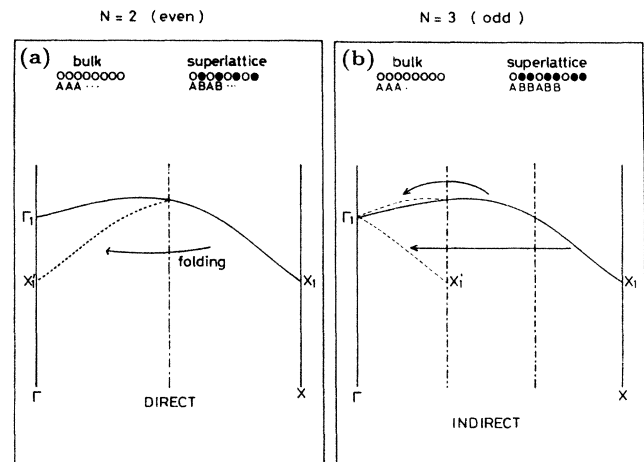

FIG. 3. Calculated band structure of GaP/AlP monolayer superlattice. Calculation includes the second-nearest-neighbor interactions. The valence-band discontinuity is assumed to be (a) $\Delta E_v = 0.00$ eV, (b) $\Delta E_v = -0.46$ eV. The dotted line represents the lowest conduction band calculated without considering second-nearest-neighbor interactions. It is found that $\Delta E_v = -0.10$ eV yields a direct-band-gap material and the qualitative feature is similar to the case in (a).

FIG. 4. Conceptual description of the indirect-to-direct transition due to the zone-folding effect. Typical cases are shown for (a) $N = 2$ and (b) $N = 3$. The former becomes a direct-band-gap material, while the latter remains an indirect-band-gap material. N is the number of sublayers in a superlattice period.
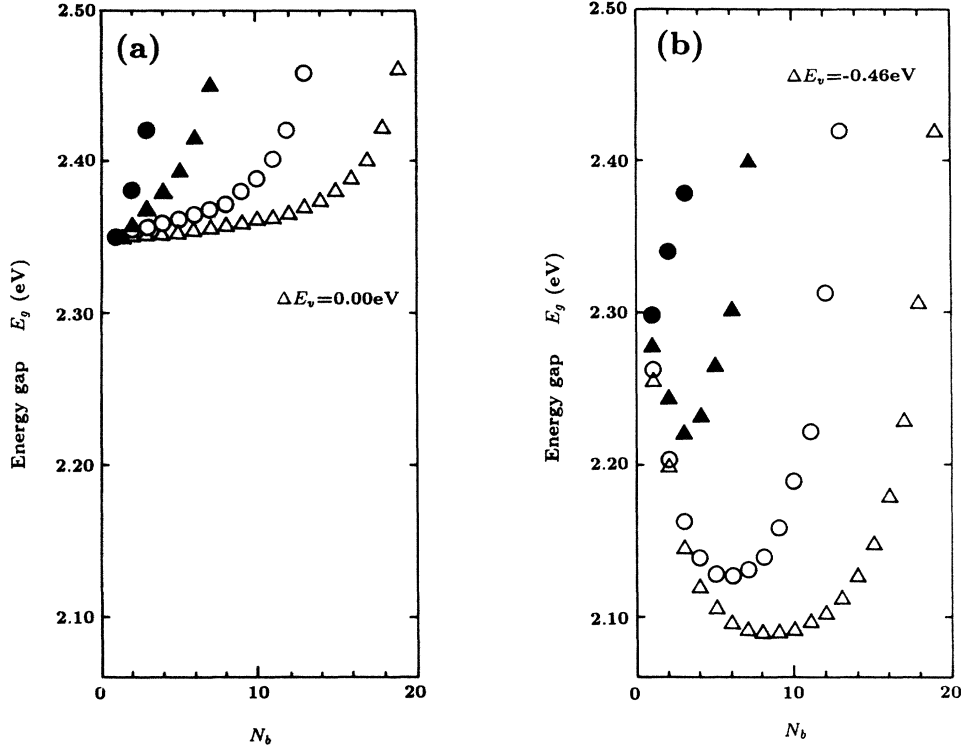
FIG. 5. Calculated energy gap of the GaP/AlP superlattice at the Γ point for the cases (a) $\Delta E_v = 0.00$ eV, (b) $\Delta E_v = -0.46$ eV. The results are presented for all combinations of numbers of GaP sublayers (N_a) and AlP sublayers (N_b) in a period under the conditions of $N = 4$ (●), 8 (▲), 14 (○), and 20 (△). The feature in the case of $\Delta E_v = -0.10$ eV is similar to the case in (a).

tice. Further discussion on this point will be given later.

The calculated energy gap at the Γ point is shown in Fig. 5 as a function of the AlP sublayer number N_b when $N = 4, 8, 14$ and $N = 20$ for two cases of (a) $\Delta E_v = 0.00$ and (b) -0.46 eV. For the monolayer superlattice ($N_a = N_b = 1$), the calculated energy gap is 2.360 and 2.271 eV corresponding to cases (a) and (b), respectively. It can be seen from Fig. 5(a) that the energy gap increases monotonically as N_b increases for every value of N. However, case (b) is definitely different from case (a). In Fig. 5(b), although the energy gap increases the value of N_b increases in the case of $N = 4$, in larger period superlattices ($N = 6, 8, 10, 12, \ldots$), the energy gap takes a minimum at some $N_b(\neq 1)$. This can be explained as follows. In larger period superlattices, the superlattice having small N_b/N_a is virtually GaP bulk crystal, and the energy gap takes a value close to that of GaP ($E_g = 2.35$ eV). On the other hand, the superlattice having large N_b/N_a is virtually AlP ($E_g = 2.50$ eV). Between those two limiting situations, the energy difference between the bottom of the AlP conduction band and the top of the GaP valence band acts as a quasienergy gap ($E_g^{\text{quasi}} = 2.04$ eV). Thus, new materials can be synthesized, whose energy gaps can be tailored by changing the thickness of the constituent materials.

III. OPTICAL PROPERTIES OF THE SUPERLATTICE

The optical transition is not always allowed even in a direct-band-gap material. It is necessary to estimate the optical properties as well as the electronic structure of the superlattice to evaluate the optical activity of the material. In this section the oscillator strength at the Γ point is calculated in order to evaluate the optical properties of the superlattice. The oscillator strength at the Γ point is calculated by using the formula[17]

$$f = \frac{2}{m\hbar\Delta\omega} | \langle \Gamma_c | M | \Gamma_v \rangle |^2 , \qquad (3.1)$$

where $M = \exp(i\mathbf{K}\cdot\mathbf{r})p$, $\hbar\Delta\omega$ is the gap energy at the Γ point, $\mathbf{K}$ is the photon wave vector, m is the free-electron mass, and p is the momentum operator. For the numerical evaluation of the formula, the atomic radial wave function obtained by a Herman and Skillman[18] type program is employed. Details of the calculation are given in Appendix B. The calculated values of oscillator strength are shown in Figs. 6(a) and 6(b) for even numbers of the superlattice period N under the condition of $N \leq 20$ corresponding to $\Delta E_v = 0.00$ and -0.46 eV, respectively. Even numbers of N are employed because the Γ-point energy of the superlattice would otherwise always be higher than the M-point energy. Only the maximum (○) and the minimum (△) values of the oscillator strength are plotted as a function of the superlattice period N, when (N_a, N_b) combinations are varied. The oscillator strength of the transition between Γ_{1c} and Γ_{15v} in bulk GaP is 0.89. A larger oscillator strength is obtained in superlattices having shorter periods for all three values of ΔE_v. Furthermore, the ratio of maximum-to-minimum values of oscillator strength gives
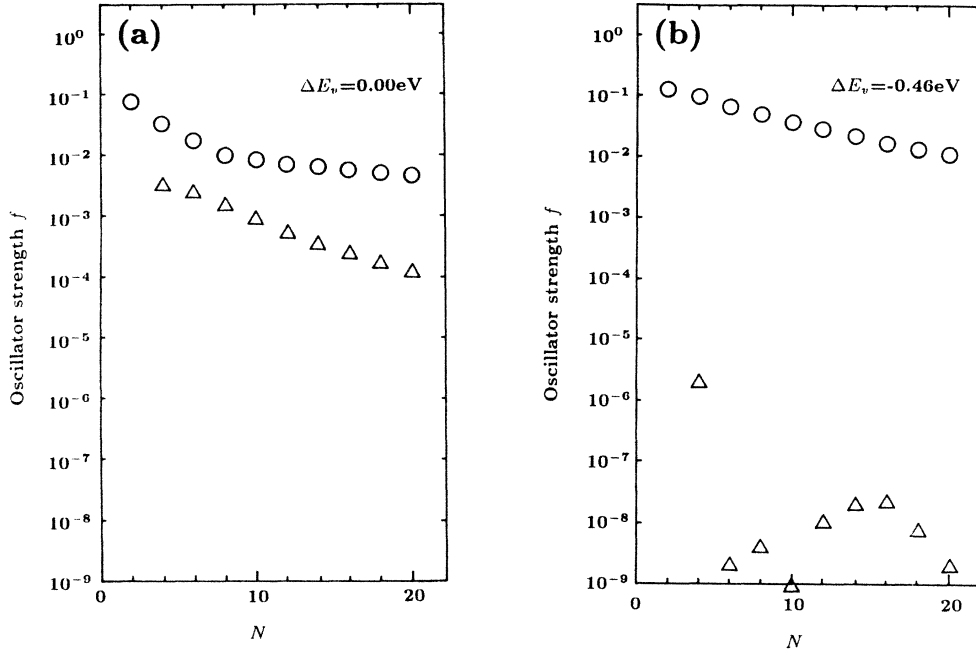
FIG. 6. Calculated oscillator strength at the Γ point versus the superlattice period N. Two cases are shown corresponding to the value of the valence-band discontinuity ΔE_v as (a) $\Delta E_v = 0.00$ eV, (b) $\Delta E_v = -0.46$ eV. Among all combinations of (N_a, N_b), only the maximum ($\bigcirc$) and minimum ($\triangle$) values of the oscillator strength are presented for a given N. For the case of $\Delta E_v = -0.10$ eV, the feature is quite similar to the case in (a). N_a and N_b stand for the number of GaP and AlP sublayers included in a superlattice period, and $N = N_a + N_b$.

a measure of the permissible level for the layer-thickness fluctuation in fabricating an optical device. The ratio is about 10 to 100 in the case of $\Delta E_v = 0.00$ eV, while it takes on an extremely large value in the case of $\Delta E_v = -0.46$ eV. It can also be seen that the maximum oscillator strength is larger in the case of $\Delta E_v = -0.46$ eV than the other two ΔE_v values. The features in the case of $\Delta E_v = -0.10$ eV are quite similar to those of $\Delta E_v = 0.00$ eV. The N_b dependence of oscillator strength is presented in Figs. 7(a) and 7(b) for $N = 20$, corresponding to $\Delta E_v = 0.00$ and -0.46 eV, respectively. It can be seen from the figure that the oscillator strength is generally larger in (odd,odd) combinations of (N_a, N_b) than in (even,even) combinations. Two groups of points can be seen in each figure, corresponding to the (odd,odd) and (even,even) combinations. A much larger difference between two groups is obtained for the case of $\Delta E_v = -0.46$ eV than for the case of $\Delta E_v = 0.00$ eV. In this respect also, the features in the case of $\Delta E_v = -0.10$ eV are similar to those of $\Delta E_v = 0.00$ eV.

Simple perturbation theory can explain these results qualitatively. The momentum needed in the indirect optical transition is supplied from the superlattice potential through a scattering process. Two possible paths of indirect optical transitions, denoted by (i) and (ii), are shown in Fig. 8. In the case of an ideal square-well-shaped potential of a superlattice having an even number of sublayers in a unit period, the oscillator strength is calculated as

$$f \propto \left| \frac{V_+}{\Delta_+} + \frac{V_-}{\Delta_-} \right|^2 , \qquad (3.2)$$

with

$$V_\pm = \begin{cases} (4V_\pm^{(0)}/N\pi)\sin(\pi N_b/2) & \text{if } N \text{ is even} , \\ 0 & \text{if } N \text{ is odd} , \end{cases} \qquad (3.3)$$

where, $V_+^{(0)}$ ($V_-^{(0)}$) is the potential height for an electron (hole), and Δ_+ (Δ_-) is the conduction- (valence-) band energy difference between the Γ and X points of the well layer material. The first term of Eq. (3.2) corresponds to path (i), and the second term to path (ii). Equation (3.2) shows that the oscillator strength is zero when the superlattice has an odd number of sublayers in a unit period. It can be also seen that the oscillator strength increases as the superlattice period N decreases. These results confirm the trend seen in Fig. 6. Furthermore, Eq. (3.3) implies that the oscillator strength is always zero for (even,even) combinations of (N_a, N_b). This is a consequence of assuming an ideal square-well-shaped potential. Actually, the shape of the superlattice potential deviates from the ideal square-well shape, so that the oscillator strength takes on a finite value. This tendency is reflected in Fig. 7 by the fact that the (odd,odd) combinations have a larger oscillator strength than the (even,even) combinations. The difference between Figs. 7(a) and 7(b) can also be explained in terms of the shape and amplitude of the superlattice potential. It can be easily seen from Eqs. (3.2) and (3.3) that a larger superlattice potential height yields a larger oscillator strength. The conduction-band discontinuity ΔE_c is 0.15 eV for the case of $\Delta E_v = 0.00$ eV, while ΔE_c is -0.31 eV for the case of $\Delta E_v = -0.46$ eV. The potential heights $V_+^{(0)}$ and $V_-^{(0)}$ are both larger in the case of $\Delta E_v = -0.46$ eV
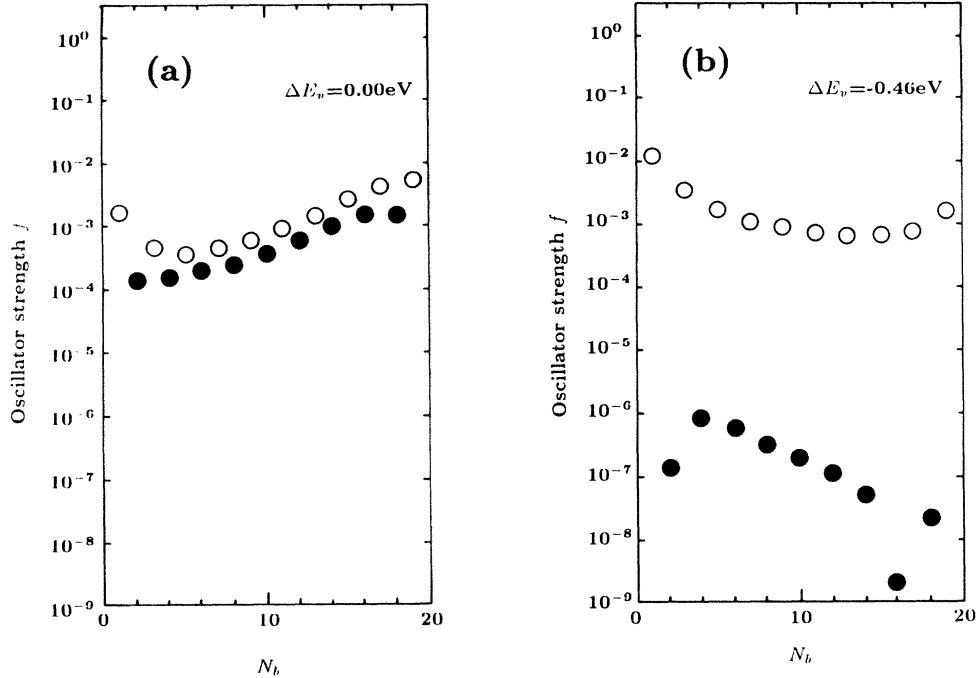
FIG. 7. N_b dependence of the calculated oscillator strength for the case of $N = 20$. Two cases are shown corresponding to the value of the valence-band discontinuity ΔE_v as (a) $\Delta E_v = 0.00$ eV, (b) $\Delta E_v = -0.46$ eV. In this case also, the feature in the case of $\Delta E_v = -0.10$ eV is quite similar to (a). The open and solid circles correspond to the (odd,odd) and (even,even) combinations of (N_a, N_b), respectively. N_a and N_b mean the same as in Fig. 6.

than in the case of $\Delta E_v = 0.00$ eV, and the potential can have a sharply formed interface leading to a larger value of maximum oscillator strength and a larger maximum-to-minimum ratio which explain the features in Fig. 6. However, the shape of the potential is not so simple. Especially in the shorter-period superlattice, this effect plays an even more significant role exceeding the limits of simple perturbation theory.

When designing materials, it is important to know the (N_a, N_b) combination which yields the maximum oscillator strength for a given N. For the case of $N = 20$, for example, such combinations are (1,19) and (19,1) for $\Delta E_v = 0.00$ and -0.46 eV, respectively. This feature can be explained qualitatively in terms of the spatial distribution of the wave function. In the following, we consider mainly superlattices having a larger period because
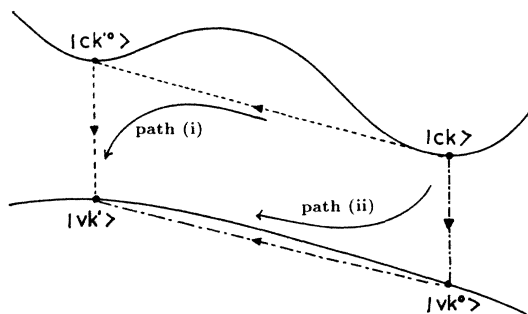

FIG. 8. Schematic diagram of the indirect optical transition based on the perturbation theoretical viewpoint. $|ck\rangle$ and $|vk'\rangle$ denote the Bloch states of the conduction and valence bands, respectively.

the qualitative interpretation becomes easier. In the indirect optical transition, the wave vector must be supplied through potential scattering at the interface, and thus the carrier distribution affects the scattering rate and the resulting oscillator strength. Since the carriers are scattered at the interface in the indirect optical transition, it is advantageous for the carriers to localize near the interface. It is reasonable to expect that a thinner well layer yields a larger oscillator strength because the carriers tend to localize at the well layer and are scattered more strongly at the interface. In Fig. 7(a), except for very small N_a, it seems that AlP-rich superlattice yields larger oscillator strength in the case of $\Delta E_v = 0.00$ eV, and a similar feature is obtained in the case of $\Delta E_v = -0.10$ eV. This is a consequence of the fact that GaP is the well layer for both electrons and holes, in the case of $\Delta E_v = 0.00$ and -0.10 eV. However, GaP is the well layer for holes and AlP is the well layer for electrons in the case of $\Delta E_v = -0.46$ eV. Consequently, the N_b dependence is not so simple in this case. It can thus be expected that a larger oscillator strength will be obtained in both the AlP-rich and GaP-rich cases, which yield thin well layers for holes and electrons, respectively.

To clarify these features, the distribution of the wave function in the superlattice is investigated. First, results for the case of $\Delta E_v = -0.46$ eV are presented in Fig. 9. Figure 9(a) represents the distribution of wave function (squared modulus of the envelope function) at the bottom of the conduction band for the superlattice having 19 GaP sublayers and one AlP sublayer in a period, and Fig. 9(b) represents the distribution at the top of the
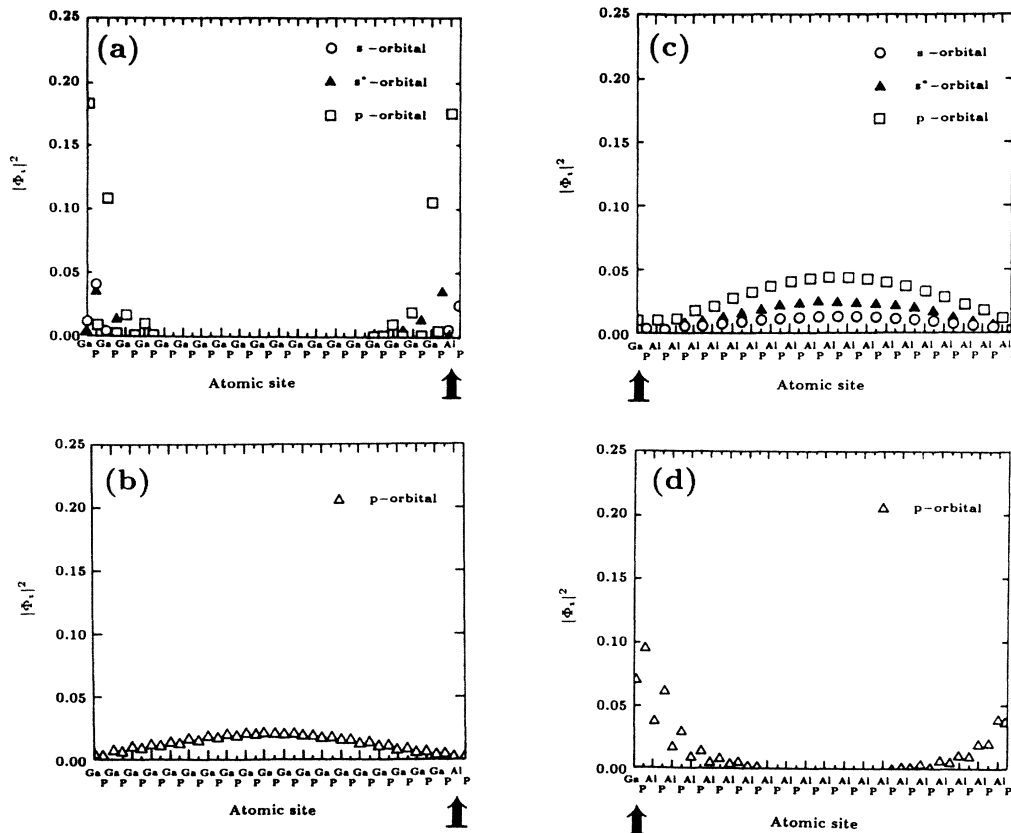
FIG. 9. Squared modulus of the envelope function in the (N_a, N_b) GaP/AlP superlattice for the case of $\Delta E_v = -0.46$ eV. Four cases are shown corresponding to (a) bottom of the conduction band for $(N_a, N_b) = (19,1)$ superlattice, (b) top of the valence band for (19,1) superlattice, (c) bottom of the conduction band for (1,19) superlattice, (d) top of the valence band for (1,19) superlattice. The horizontal axis shows the atomic species for each site in a period of superlattice. The arrows show the sites where thinner layer lies, for each case. The circles, squares, etc. correspond to the squared modulus associated with the atomic s orbital, p orbital, etc., as indicated in the figure.

valence band. It can be seen that electrons tend to localize at the AlP layer while holes tend to localize at the middle of the GaP layer. Figures 9(c) and 9(d) show similar results for a superlattice having one GaP sublayer and 19 AlP sublayers in a period. In this case, the situation is reversed. These localization features are the final results of the potential scattering of the carriers caused by the superlattice structure. It can be seen that the sharply localized wave function exhibits a marked influence of the superlattice potential. In this sense, both cases are thought to yield large oscillator strength, and this can be confirmed in Fig. 7(b). In the case where N_a and N_b are both larger, the influence of the interfaces is thought to be weak, because electrons and holes are both widely spread in GaP and AlP layers. This is reflected in the small oscillator strength for the cases where $N_a \simeq N_b$ in Fig. 7(b). Figure 10 shows the results for the case of $\Delta E_v = 0.00$ eV. Figure 10(a) represents the distribution of the wave function at the bottom of the conduction band for the same superlattice as in Figs. 9(a) and 9(b), and Fig. 10(b) represents that at the top of the valence band. In this case, however, the localization feature of the wave function is not so clear. Especially, the wave function at the top of the valence band is al-

most completely delocalized in both the GaP and AlP layers. This is reasonable because there is no potential barrier with respect to the valence band. However, the behavior of the wave function at the bottom of the conduction band is quite strange because it is not as strongly localized in the GaP layer as expected. This behavior is somewhat peculiar to the $(N_a, N_b) = (19,1)$ combination, because in other GaP-rich cases (e.g., $N_a = 18$, $N_b = 2$), the wave functions are apparently localized in the GaP layer. This is thought to be the reason for the strange behavior of the oscillator strength of the $(N_a, N_b) = (19,1)$ superlattice in Fig. 7(a). Figures 10(c) and 10(d) correspond to a superlattice having one GaP sublayer and 19 AlP sublayers in a period. In this case, the situation is easy to interpret. The features of valence band in Fig. 10(d) are very similar to those in Fig. 10(b), but the features of conduction band in Fig. 10(c) are much different from those in Fig. 10(a) and the wave function is strongly localized near the GaP layer which is the well layer for the electron. For shorter-period superlattices (e.g., $N = 2, 4, \ldots$) these interpretations cannot be applied because the carrier localization and the scattering effect at the interfaces are not related to each other in a simple manner.
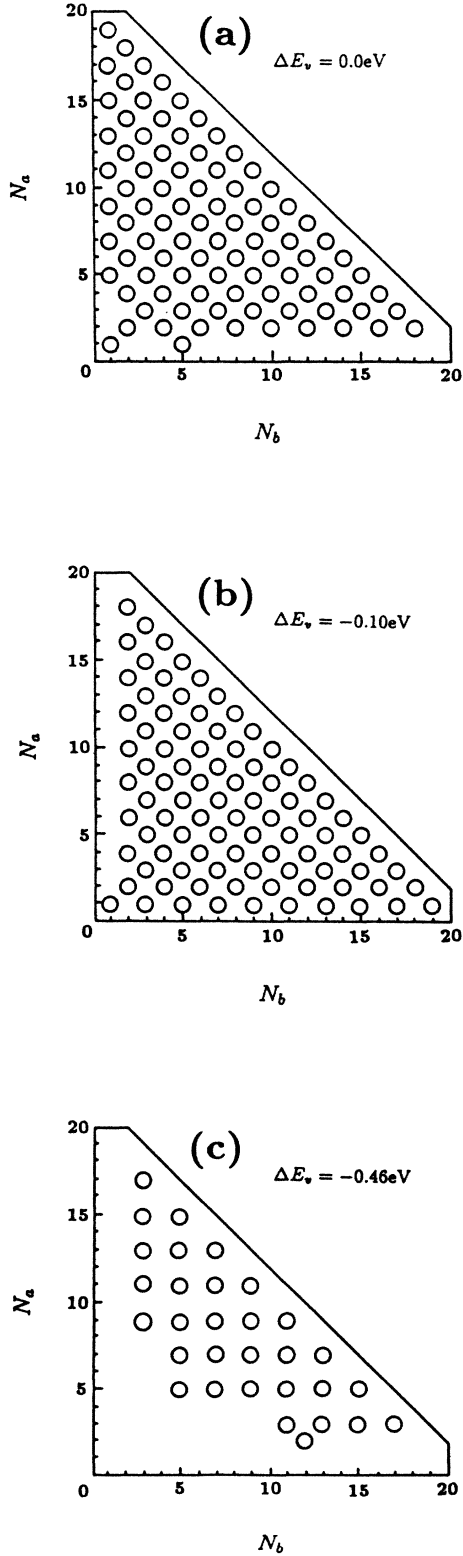
FIG. 10. Squared modulus of the envelope function in the GaP/AlP superlattice for the case of $\Delta E_V = 0.00$ eV. Notations are the same as in Fig. 9.

IV. STRUCTURALLY-INDUCED INDIRECT-TO-DIRECT TRANSITION

As mentioned in Sec. II, it is still not clear whether the superlattice is a direct- or indirect-band-gap material, seen if the conduction-band minimum is folded at the Γ point. In order to clarify the position of the superlattice's conduction-band minimum, the band structure over the entire Brillouin zone is calculated. In Fig. 11, the (N_a, N_b) combinations which yield the conduction-band minimum at the Γ point are given by open circles under the condition that $N \leq 20$. Three cases are shown corresponding to the values of valence-band discontinuity ΔE_v of 0.00, -0.10, and -0.46 eV. The energy band structure of the superlattice is quite sensitive to the choice of ΔE_v, and this results in the different combinations of (N_a, N_b) which make the superlattice in a direct-band-gap material. For type-I superlattices, an interesting feature can be seen when Figs. 11(a) and 11(b) are compared. In Fig. 11(a) the combinations which make the superlattice of even N an indirect-band-gap material are restricted to those having only one GaP sublayer in a period, while in Fig. 11(b), such combinations are restricted to those having only one AlP sublayer in a period. Summarizing the cases where GaP/AlP superlattices are of type I, the superlattices having small and odd N_a and N_b are useful for application to optical devices, because almost all of them are

direct-band-gap materials and have large oscillator strength, as shown in Fig. 6.

As for the case of type-II superlattices [Fig. 11(c)], shorter-period superlattices of even N remain indirect-band-gap materials having their conduction-band minimum at the edge of the Brillouin zone in the x or y direction. Larger-period superlattices can be classified into four types depending on the band structure. One is a superlattice which has thin GaP or AlP layers and has the conduction-band minimum at the edge of the Brillouin zone in the x or y direction, like shorter-period superlattices. Another has an (odd,odd) combination for (N_a, N_b), and the conduction-band minimum is at the Γ point, assuring a direct optical transition. Adding them, there is an (even,even) combination for (N_a, N_b) having the conduction-band minimum at the edge of the Brillouin zone in the z direction. This type of superlattice is not seen in the cases of $\Delta E_v = 0.00$ and -0.10 eV. The other type has an odd N, and has the conduction-band minimum at the edge of the Brillouin zone in the z direction.

Summarizing the case of type-II superlattices, it would appear that GaP/AlP superlattices are also as advantageous for optical devices as type-I superlattices, although the oscillator strength is a little smaller. In any case, from the results given above, the valence-band discontinuity between GaP and AlP can be evaluated experimentally by measuring the optical properties of the superlattice.

TABLE II. Elastic moduli of GaP and AlP bulk crystals (in 10^{11} dyn cm^{-2}).

	c_{11}	c_{12}	c_{44}
GaP	14.14	6.40	7.03
AlP	13.20	6.30	6.15

FIG. 11. Phase diagram for the indirect-to-direct transition of the (N_a,N_b) GaP/AlP superlattice with respect to the layer-thickness combination. The circles represent the combinations of (N_a,N_b) which yield direct-band-gap materials. Three cases are shown corresponding to the value of the valence-band discontinuity ΔE_v: (a) $\Delta E_v = 0.00$ eV, (b) $\Delta E_v = -0.10$ eV, (c) $\Delta E_v = -0.46$ eV.
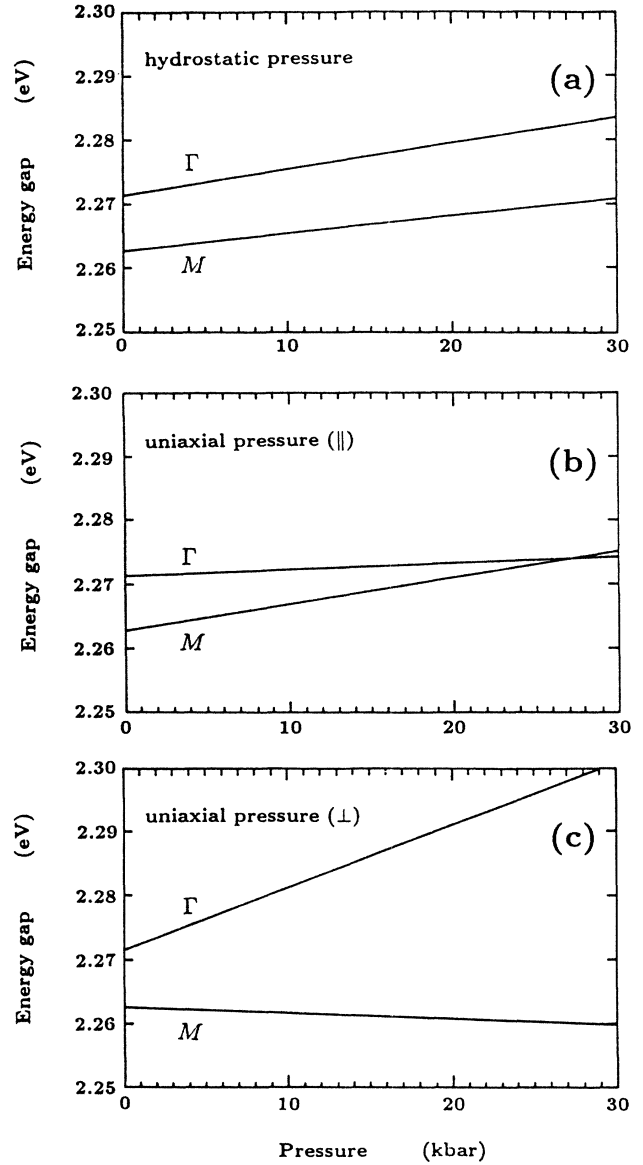
FIG. 12. Pressure dependence of the energy gap in the GaP/AlP monolayer superlattice for the case of $\Delta E_v = -0.46$ eV. The energy gaps between the top of the valence band and the local minima of the conduction band at the Γ point (direct-band gap) and at the M point (indirect-band gap) are denoted by Γ and M, respectively. Three cases of pressure application are presented: (a) hydrostatic pressure, (b) uniaxial pressure parallel ($\parallel$) to the layers, (c) uniaxial pressure perpendicular ($\perp$) to the layers.

V. PRESSURE-INDUCED
INDIRECT-TO-DIRECT TRANSITION

In Sec. III the indirect-to-direct transition in the GaP/AlP superlattices caused by the structural modulation of the potential is investigated. It is found that the indirect-to-direct transition does not occur in short-period superlattices having large oscillator strength in the case of $\Delta E_v = -0.46$ eV. These superlattices are not favorable for application to optical devices. In order to examine the possibility of inducing the indirect-to-direct transition in these superlattices, the effect of pressure is investigated. Applied pressure induces changes in the electron transfer-matrix elements primarily through changes of interatomic distances in the constituent materials, and consequently modifies the electronic band

structure. Up to now, the actual band structure has not yet been reported for AlP under pressure, and thus the empirical band-fitting method cannot be applied for the calculation.

In this work, by assuming the d^{-2} rule[19] for the interaction matrix elements, and using the reported elastic moduli,[20,21] the pressure dependence of the interaction matrix elements are derived. Details of the calculation are given in Appendix C. The elastic moduli used here are tabulated in Table II, and are assumed to be independent of the pressure in the range up to 30 kbar.

Figure 12 shows the pressure dependence of the energy gaps between the valence-band top and two conduction-band local minima (Γ and M points) for the monolayer superlattice in the case of $\Delta E_v = -0.46$ eV, which has its conduction-band minimum at the M point.
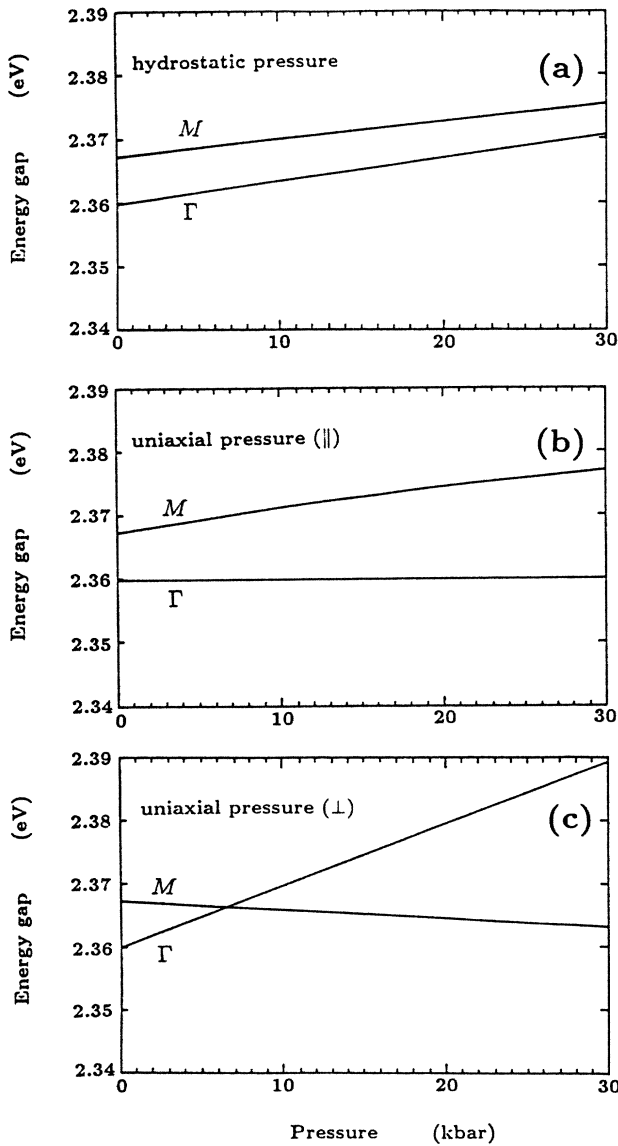

FIG. 13. Pressure dependence of the energy gap in the GaP/AlP monolayer superlattice for the case of $\Delta E_v = 0.00$ eV. Notations are the same as in Fig. 12.
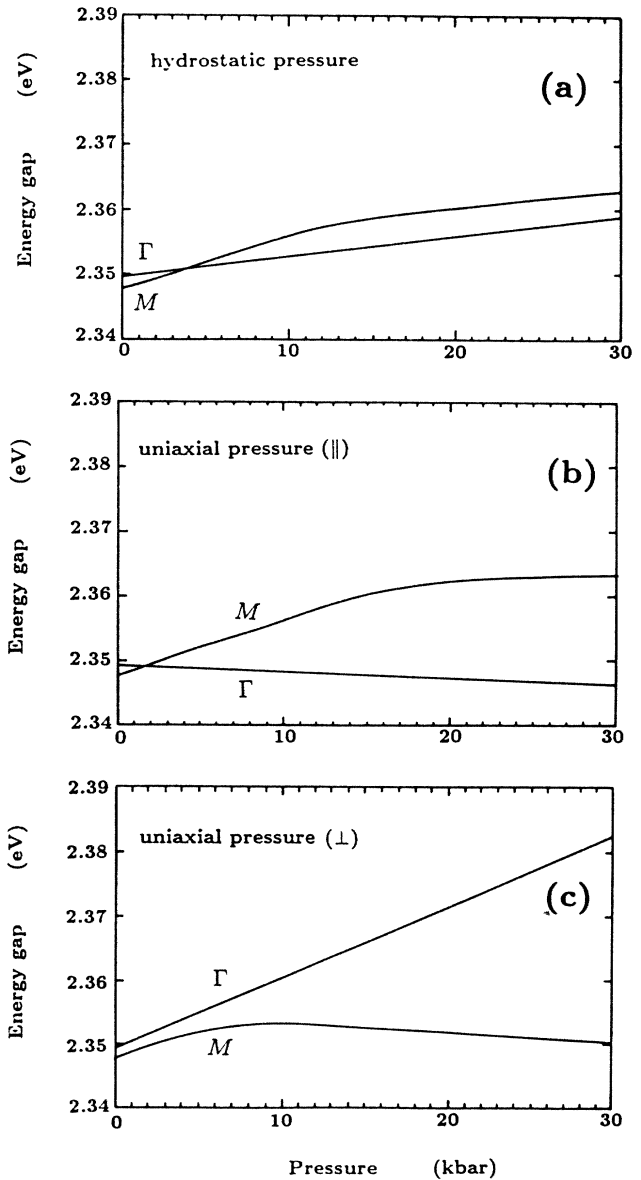
FIG. 14. Pressure dependence of the energy gap in the $(N_a, N_b) = (3,1)$ GaP/AlP superlattice for the case of $\Delta E_v = 0.00$ eV. Notations are the same as in Fig. 12.

Three cases are shown in the figure corresponding to hydrostatic pressure and uniaxial pressure applied parallel ($\parallel$) and perpendicular ($\perp$) to the layers. In the case of the uniaxial pressure ($\parallel$), the M-point energy rises faster than the Γ-point energy as the pressure is increased, and the indirect-to-direct transition occurs above 27 kbar. In the other two cases, however, the M-point energy does not become larger than the Γ-point energy and the indirect-to-direct transition cannot be expected.

Figure 13 shows similar results for the case of $\Delta E_v = 0.00$ eV. In this case the superlattice is a direct-band-gap material and the direct-to-indirect transition is induced by uniaxial pressure ($\perp$) above 6 kbar. In this case the pressure dependence of the direct- and indirect-band gaps are quite similar to the case of $\Delta E_v = -0.46$ eV. For the other two types of applied pressure, the direct-to-indirect transition does not occur in the range up to 30 kbar.

Similar calculations are also made for the superlattice having three sublayers of GaP and one sublayer of AlP in a period for the case of $\Delta E_v = 0.00$ eV. This superlattice is an indirect-band-gap material as shown in Fig. 11, and the indirect-to-direct transition is induced by applying uniaxial pressure ($\parallel$) above 2 kbar or hydrostatic pressure above 4 kbar. These features are shown in Fig. 14.

As shown above, the indirect-to-direct and the direct-to-indirect transitions can be induced by applying pressure in the appropriate directions. Figures 15 and 16 show the features of those transitions corresponding to $\Delta E_v = -0.46$ and 0.00 eV, respectively. In the calculation, a pressure of 30 kbar is assumed to be applied to the superlattices for all three types of pressure. The following general features can be seen from Fig. 15. (1) Uniaxial pressure ($\parallel$) stimulates an indirect-to-direct transition. (2) Uniaxial pressure ($\perp$) stimulates the direct-to-indirect transition. By applying a uniaxial pressure ($\perp$) of 30 kbar, all superlattices can be turned into indirect-band-gap materials under the condition of $N \leq 20$. Hydrostatic pressure induces both direct-to-indirect and indirect-to-direct transition in the cases of $(N_a,N_b)=(2,12)$ and $(3,9)$, respectively. In Fig. 16, similar results can be seen for two types of uniaxial pressure, but hydrostatic pressure stimulates the indirect-to-direct transition but not the direct-to-indirect transition.

Summarizing the features of pressure-induced indirect-to-direct transition, it is quite advantageous to apply uniaxial pressure parallel to the layers in order to induce indirect-to-direct transitions in short-period superlattices having large oscillator strength. On the other
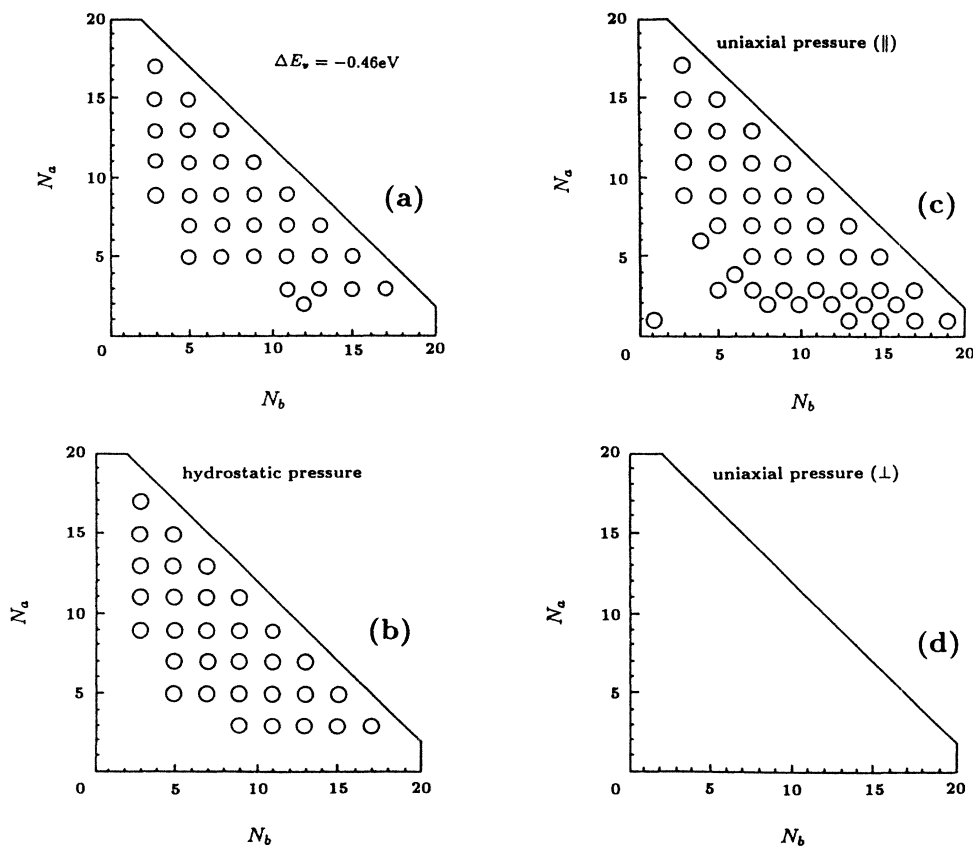

FIG. 15. Phase diagram of the pressure-induced indirect-to-direct and direct-to-indirect transition of the (N_a,N_b) GaP/AlP superlattice for the case of $\Delta E_v = -0.46$ eV. The circles represent combinations of (N_a,N_b) which yield direct-band-gap materials. Four cases of pressure application are presented: (a) without pressure, (b) 30-kbar hydrostatic pressure, (c) 30-kbar uniaxial pressure parallel ($\parallel$) to the layers, (d) 30-kbar uniaxial pressure perpendicular ($\perp$) to the layers.
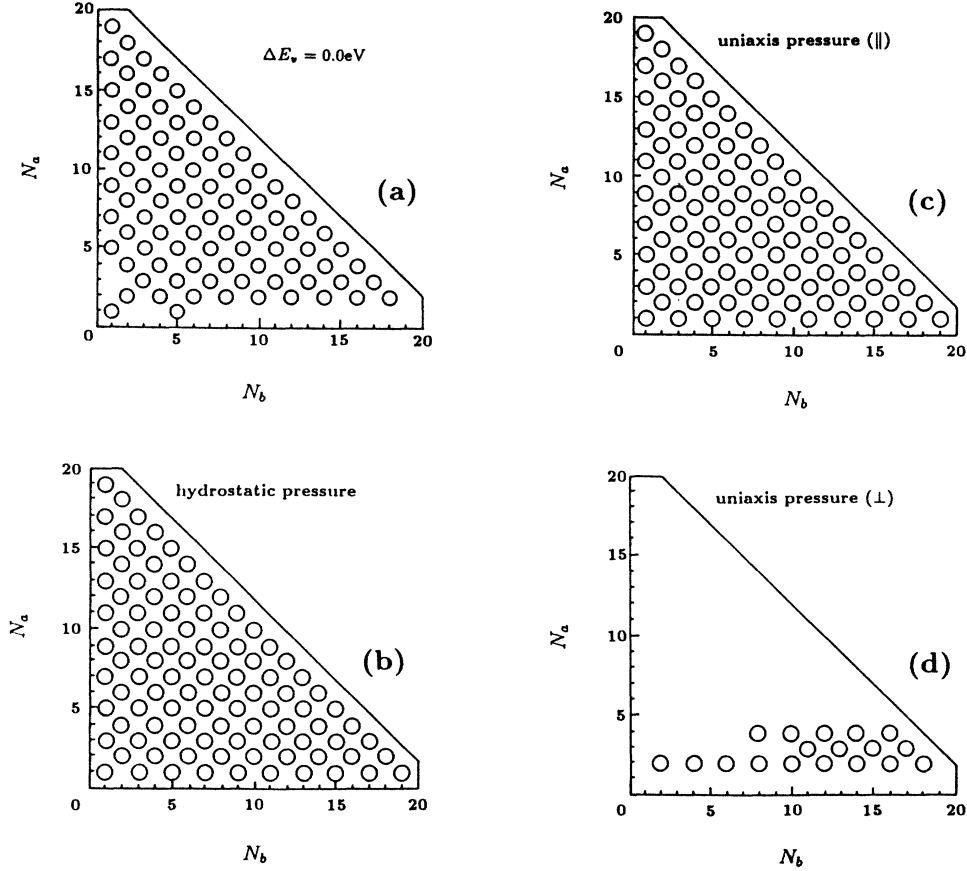
FIG. 16. Phase diagram of the pressure-induced indirect-to-direct and direct-to-indirect transition of the GaP/AlP superlattice for the case of $\Delta E_v = 0.00$ eV. Notations are the same as in Fig. 15.

hand, uniaxial pressure applied perpendicular to the layers tends to stimulate the direct-to-indirect transition, and it is not useful for enhancing the optical activity.

VI. SUMMARY AND CONCLUSION

This paper investigated the general aspects of the optical properties as well as the electronic structure of the superlattice which is made of indirect-band-gap semiconductors, referring mainly to the case of the GaP/AlP superlattice. This superlattice exhibits rather interesting features which differ greatly from those of the original materials with respect to optical properties as well as in the electronic structure. Also, pressure-induced indirect-to-direct and direct-to-indirect transitions are investigated as an example of the effect of external perturbation applied to the superlattice. The nature of this superlattice is clarified as follows. (1) The energy gap of the superlattice can be adjusted by changing the layer-thickness combination in a superlattice period. (2) The indirect-to-direct transition can be induced by the superlattice potential. This transition is quite sensitive to the band discontinuity. (3) Larger oscillator strength can be obtained in shorter-period superlattices, which are quite promising for application to optical devices operating in

the visible-light region. (4) Oscillator strength is sensitively dependent on the superlattice structure and the band discontinuity. (5) Pressure application yields significant changes in the electronic structure and induces either indirect-to-direct or direct-to-indirect transition.

The present theoretical formulation is quite general and is thus applicable to the band-structure calculation of superlattices composed of any combination of zinc-blende-type indirect- and/or direct-band-gap semiconductors, once the relevant parameters of the sp^3s^* tight-binding scheme have been established. The sensitivity of the electronic structure and optical properties of these superlattices to the layer-thickness combination and to the applied pressure makes it possible to design a material having a desirable gap energy and oscillator strength. Most of the indirect-band-gap III-V compound semiconductors have band-gap energies in the visible-light region. Thus the structurally-induced optical transition holds a great promise for application to optical devices operating in the visible-light region. The possibility of the band-structure designing of applying pressure is quite interesting. However, it is much more desirable from the viewpoint of device application that the externally applied pressure is replaced by a built-in strain

field. In the case of the GaP/AlP superlattice, the lattice constants are most matched and the induced strain field is small. On the other hand, in the strained-layer superlattice, the intrinsic strain field can modify the band structure significantly. In fact, an Si/Ge strained-layer superlattice was fabricated, and several structurally induced optical transitions were identified experimentally.[22,23] Similarly, in the case of compound semiconductors, a suitable combination of indirect-band-gap materials will yield a built-in strain field and induce a favorable indirect-to-direct transition. The possibility of designing the band structure suggested here will open the way to applying superlattices composed of indirect-band-gap semiconductors to novel functional devices.

ACKNOWLEDGMENTS

APPENDIX A: ELECTRONIC STRUCTURE CALCULATION OF THE SUPERLATTICE

The following presents the details of the electronic structure calculation. The suffixes c (c') and a (a') stand for the cation and anion of the A (B) material which correspond to Ga (Al) and P (P) in the GaP/AlP superlattice. The wave function corresponding to the atoms in the mth sublayer of A is denoted by $|\phi^b(m)\rangle$, and that corresponding to the nth sublayer of B is denoted by $|\phi^{b'}(n)\rangle$, where b (b') takes c and a (c' and a') corresponding to the cation plane and the anion plane in which the atom lies. The wave function of the superlattice can be written in terms of these basis functions as

$$|\psi\rangle = \sum_{\substack{m \in A \\ b=c,a}} f^b(m)\,|\phi^b(m)\rangle + \sum_{\substack{m' \in B \\ b'=c',a'}} f^{b'}(n)\,|\phi^{b'}(n)\rangle \ , \tag{A1}$$

where $f^b(m)$ and $f^{b'}(n)$ are expansion coefficients. Thus the Hamiltonian can be represented by considering the first- and second-nearest-neighbor interactions as

$$H = \begin{bmatrix}
H_c & V_{\rm I}^A & U_{cc} & 0 & \cdots & 0 & 0 & 0 & 0 & 0 & 0 & \cdots & 0 & 0 & U_{cc'}^\dagger h_- & V_{\rm II}^{C\dagger} h_- \\
V_{\rm I}^{A\dagger} & H_a & V_{\rm II}^A & U_{aa} & \cdots & 0 & 0 & 0 & 0 & 0 & 0 & \cdots & 0 & 0 & 0 & U_{aa'}^\dagger h_- \\
U_{cc}^\dagger & V_{\rm II}^{A\dagger} & H_c & V_{\rm I}^A & \cdots & 0 & 0 & 0 & 0 & 0 & 0 & \cdots & 0 & 0 & 0 & 0 \\
0 & U_{aa}^\dagger & V_{\rm I}^{A\dagger} & H_a & \cdots & 0 & 0 & 0 & 0 & 0 & 0 & \cdots & 0 & 0 & 0 & 0 \\
\vdots & \vdots & \vdots & \vdots & \ddots & \vdots & \vdots & \vdots & \vdots & \vdots & \vdots & \ddots & \vdots & \vdots & \vdots & \vdots \\
0 & 0 & 0 & 0 & \cdots & U_{aa}^\dagger & V_{\rm I}^{A\dagger} & H_a & V_{\rm II}^D & U_{aa'} & 0 & \cdots & 0 & 0 & 0 & 0 \\
0 & 0 & 0 & 0 & \cdots & 0 & U_{cc'}^\dagger & V_{\rm II}^{D\dagger} & H_{c'} & V_{\rm I}^B & U_{cc} & \cdots & 0 & 0 & 0 & 0 \\
\vdots & \vdots & \vdots & \vdots & \ddots & \vdots & \vdots & \vdots & \vdots & \vdots & \vdots & \ddots & \vdots & \vdots & \vdots & \vdots \\
0 & 0 & 0 & 0 & \cdots & 0 & 0 & 0 & 0 & 0 & \cdots & H_{c'} & V_{\rm I}^B & U_{c'c'} & 0 \\
0 & 0 & 0 & 0 & \cdots & 0 & 0 & 0 & 0 & 0 & \cdots & V_{\rm I}^{B\dagger} & H_{a'} & V_{\rm II}^B & U_{a'a'} \\
U_{cc'} h_+ & 0 & 0 & 0 & \cdots & 0 & 0 & 0 & 0 & 0 & \cdots & U_{c'c'}^\dagger & V_{\rm II}^{B\dagger} & H_{c'} & V_{\rm I}^B \\
V_{\rm II}^C h_+ & U_{aa'} h_+ & 0 & 0 & \cdots & 0 & 0 & 0 & 0 & 0 & \cdots & 0 & U_{a'a'}^\dagger & V_{\rm I}^{B\dagger} & H_{a'}
\end{bmatrix} \tag{A2}$$

where

$$H_c \equiv \langle \phi^c(m)\,|\,H\,|\,\phi^c(m)\rangle, \quad H_a \equiv \langle \phi^a(m)\,|\,H\,|\,\phi^a(m)\rangle \ ,$$

$$H_{c'} \equiv \langle \phi^{c'}(n)\,|\,H\,|\,\phi^{c'}(n)\rangle, \quad H_{a'} \equiv \langle \phi^{a'}(n)\,|\,H\,|\,\phi^{a'}(n)\rangle \ ,$$

$$V_{\rm I}^A \equiv \langle \phi^c(m)\,|\,H\,|\,\phi^a(m)\rangle, \quad V_{\rm II}^A \equiv \langle \phi^a(m)\,|\,H\,|\,\phi^c(m+1)\rangle \ ,$$

$$V_{\rm I}^B \equiv \langle \phi^{c'}(n)\,|\,H\,|\,\phi^{a'}(n)\rangle, \quad V_{\rm II}^B \equiv \langle \phi^{a'}(n)\,|\,H\,|\,\phi^{c'}(n+1)\rangle \ , \tag{A3}$$

$$V_{\rm II}^C \equiv \langle \phi^{a'}(N)\,|\,H\,|\,\phi^c(N+1)\rangle, \quad V_{\rm II}^D \equiv \langle \phi^a(N_a)\,|\,H\,|\,\phi^{c'}(N_a+1)\rangle \ ,$$

$$U_{cc} \equiv \langle \phi^c(m)\,|\,H\,|\,\phi^c(m+1)\rangle, \quad U_{aa} \equiv \langle \phi^a(m)\,|\,H\,|\,\phi^a(m+1)\rangle \ ,$$

$$U_{cc'} \equiv \langle \phi^c(N_a)\,|\,H\,|\,\phi^{c'}(N_a+1)\rangle, \quad U_{aa'} \equiv \langle \phi^a(N_a)\,|\,H\,|\,\phi^{a'}(N_a+1)\rangle \ ,$$

and

$$h_+ = \exp\left[\frac{+iNk_zd}{2}\right], \quad h_- = \exp\left[\frac{-iNk_zd}{2}\right] \ . \tag{A4}$$

In the following calculation, the sp^3s^* bases are employed, and then each matrix element given in Eq. (A3) is a 5×5 matrix. The 5×5 submatrices take the following form:

$$H_{b(b')} \equiv H_{b(b')}^{(0)} + U_{b(b')} \, , \tag{A5}$$

$$H_{b(b')}^{(0)} \equiv \begin{pmatrix} E_s^{b(b')} & 0 & 0 & 0 & 0 \\ 0 & E_p^{b(b')} & 0 & 0 & 0 \\ 0 & 0 & E_p^{b(b')} & 0 & 0 \\ 0 & 0 & 0 & E_p^{b(b')} & 0 \\ 0 & 0 & 0 & 0 & E_{s*}^{b(b)} \end{pmatrix} \, , \tag{A6}$$

$$U_{b(b')} \equiv \begin{pmatrix} 0 & 0 & 0 & 0 & 0 \\ 0 & 0 & 0 & 0 & 0 \\ 0 & 0 & 0 & 0 & 0 \\ 0 & 0 & 0 & U_{pp\pi}^{b(b')}f_3 & 0 \\ 0 & 0 & 0 & 0 & 0 \end{pmatrix} \, , \tag{A7}$$

$$V_{\rm I}^X \equiv \begin{pmatrix} V_{ss}^X g_0 & -V_{s^c p}^X g_1 & -V_{s^c p}^X g_1 & -V_{s^c p}^X g_0 & 0 \\ V_{s^a p}^X g_1 & -V_{xx}^X g_0 & V_{xy}^X g_0 & V_{xy}^X g_0 & V_{s^* a_p}^X g_1 \\ V_{s^a p}^X g_1 & V_{xy}^X g_0 & -V_{xx}^X g_0 & V_{xy}^X g_0 & V_{s^* a_p}^X g_1 \\ V_{s^a p}^X g_0 & V_{xy}^X g_1 & V_{xy}^X g_1 & -V_{xx}^x g_0 & V_{s^* a_p}^X g_0 \\ 0 & -V_{s^* c_p}^X g_1 & -V_{s^* c_p}^X g_1 & -V_{s^* c_p}^X g_0 & 0 \end{pmatrix} \, , \tag{A8}$$

$$V_{\rm II}^X \equiv \begin{pmatrix} V_{ss}^X g_2 & -V_{s^a p}^X g_3 & V_{s^a p}^X g_3 & -V_{s^a p}^X g_2 & 0 \\ V_{s^c p}^X g_3 & -V_{xx}^X g_2 & -V_{xy}^X g_2 & V_{xy}^X g_3 & V_{s^* c_p}^X g_3 \\ -V_{s^c p}^X g_3 & -V_{xy}^X g_2 & -V_{xx}^X g_2 & -V_{xy}^X g_3 & -V_{s^* c_p}^X g_3 \\ V_{s^c p}^X g_2 & V_{xy}^X g_3 & -V_{xy}^X g_3 & -V_{xx}^X g_3 & V_{s^* c_p}^X g_2 \\ 0 & -V_{s^* a_p}^X g_3 & V_{s^* a_p}^X g_3 & -V_{s^* a_p}^X g_2 & 0 \end{pmatrix} \, , \tag{A9}$$

$$U_{bb(bb')} \equiv \begin{pmatrix} 0 & 0 & 0 & 0 & 0 \\ 0 & U_{pp\pi}^{bb(bb')}f_1 & 0 & 0 & 0 \\ 0 & 0 & U_{pp\pi}^{bb(bb')}f_2 & 0 & 0 \\ 0 & 0 & 0 & 0 & 0 \\ 0 & 0 & 0 & 0 & 0 \end{pmatrix} \, , \tag{A10}$$

where

$$g_0 = \cos(k_x d/4)\cos(k_y d/4)$$
$$\quad -\sin(k_x d/4)\sin(k_y d/4) \, ,$$

$$g_1 = i\,[\sin(k_x d/4)\cos(k_y d/4)$$
$$\quad +\cos(k_x d/4)\sin(k_y d/4)] \, ,$$

$$g_2 = \cos(k_x d/4)\cos(k_y d/4)$$
$$\quad +\sin(k_x d/4)\sin(k_y d/4) \, ,$$

$$g_3 = i\,[\sin(k_x d/4)\cos(k_y d/4)$$
$$\quad -\cos(k_x d/4)\sin(k_y d/4)] \, , \tag{A11}$$

$$f_1 = \tfrac{1}{2}\cos(k_y d/2) \, ,$$

$$f_2 = \tfrac{1}{2}\cos(k_x d/2) \, ,$$

$$f_3 = \cos(k_x d/2)\cos(k_y d/2) \, ,$$

and b takes c or a, b' takes c' or a', and X takes A, B, C, or D corresponding to four combinations of cation and anion. "A" represents the A-compound semicon-

ductor made of c and a atoms; "B", the B-compound semiconductor made of c' and a'; "C", the compound semiconductor made of c and a'; and "D" represents the compound semiconductor made of c' and a. For GaP/AlP superlattices, C and D correspond to GaP and AlP, respectively. The lattice constant is denoted by d, which is assumed to have the same values in A- and B-compound semiconductors. The lattice constants of GaP and AlP are 5.451 and 5.467 Å, respectively, and the lattice mismatch between them is about 0.3%, whereas that between GaAs and AlAs is about 0.1%. Therefore it can be said that the GaP/AlP superlattice is nearly lattice matched. If perfectly-lattice-matched superlattices are needed, a slight amount of As-contained

mixed-crystal GaAsP can be used to equalize the lattice constant of GaP to that of AlP. V_I^X and V_{II}^X represent the first-nearest-neighbor interactions, and $U_{b(b')}$ and $U_{bb(bb')}$ represent the second-nearest-neighbor interactions. The second-nearest-neighbor interactions considered here are the interactions between two p_i orbitals separated by a lattice vector of $(d/2)(\pm e \pm e_k)$, where i, j, and k are the cyclic permutation of x, y, and z, and e_j is a unit vector in the jth direction. The tight-binding parameters noted above are determined by fitting the bulk band to the reference band.[13,24] The first-nearest-neighbor parameters can be determined analytically as follows, leaving the second-nearest-neighbor parameters $U_{pp\pi}^c$ and $U_{pp\pi}^a$ to be fixed later:

$$E_{s^c} = \tfrac{1}{2}[E_{\Gamma_1^c} + E_{\Gamma_1^v} + 0.8(W_{s^c} - W_{s^a})] \ , \tag{A12}$$

$$E_{s^a} = \tfrac{1}{2}[E_{\Gamma_1^c} + E_{\Gamma_1^v} - 0.8(W_{s^c} - W_{s^a})] \ , \tag{A13}$$

$$E_{p^c} = \tfrac{1}{2}[E_{\Gamma_{15}^c} + E_{\Gamma_{15}^v} - U_{pp\pi}^a - U_{pp\pi}^c + 0.6(W_{p^c} - W_{p^a})] \ , \tag{A14}$$

$$E_{p^a} = \tfrac{1}{2}[E_{\Gamma_{15}^c} + E_{\Gamma_{15}^v} - U_{pp\pi}^a - U_{pp\pi}^c - 0.6(W_{p^c} - W_{p^a})] \ , \tag{A15}$$

$$E_{s*c} = W_{s*c} + 0.2W_{s*a} \ , \tag{A16}$$

$$E_{s*a} = W_{s*a} + 0.2W_{s*c} \ , \tag{A17}$$

$$V_{ss} = -(E_{s^a}E_{s^c} - E_{\Gamma_1^c}E_{\Gamma_1^v})^{1/2} \ , \tag{A18}$$

$$V_{xx} = [(E_{p^a} + U_{pp\pi}^a)(E_{p^c} + U_{pp\pi}^c) - E_{\Gamma_{15}^c}E_{\Gamma_{15}^v}]^{1/2} \ , \tag{A19}$$

$$V_{xy} = [(E_{p^a} - U_{pp\pi}^a)(E_{p^c} - U_{pp\pi}^c) - E_{X_5^c}E_{X_5^v}]^{1/2} \ , \tag{A20}$$

$$V_{s^c p^a} = \left[(E_{s^c} - E_{X_3^v})(E_{s^c} - E_{X_3^c}) \frac{(E_{p^a} + U_{pp\pi}^a - E_{X_3^v})(E_{s*c} - E_{X_3^v}) - (E_p^a + U_{pp\pi}^a - E_{X_3^c})(E_{s*c} - E_{X_3^c})}{(E_{s*c} - E_{X_3^v})(E_{s^c} - E_{X_3^c}) - (E_{s*c} - E_{X_3^c})(E_{s^c} - E_{X_3^v})} \right]^{1/2} \ , \tag{A21}$$

$$V_{s^a p^c} = \left[(E_{s^a} - E_{X_1^v})(E_{s^a} - E_{X_1^c}) \frac{(E_{p^c} + U_{pp\pi}^c - E_{X_1^v})(E_{s*a} - E_{X_1^v}) - (E_p^c + U_{pp\pi}^c - E_{X_1^c})(E_{s*a} - E_{X_1^c})}{(E_{s*a} - E_{X_1^v})(E_{s^a} - E_{X_1^c}) - (E_{s*a} - E_{X_1^c})(E_{s^a} - E_{X_1^v})} \right]^{1/2} \ , \tag{A22}$$

$$V_{s*c p^a} = \left[(E_{p^a} + U_{pp\pi}^a - E_{X_3^c})(E_{s*c} - E_{X_3^c}) - V_{s^c p^a}^2 \frac{E_{s*c} - E_{X_3^c}}{E_{s^c} - E_{X_3^c}} \right]^{1/2} \ , \tag{A23}$$

$$V_{s*a p^c} = \left[(E_{p^c} + U_{pp\pi}^c - E_{X_1^c})(E_{s*a} - E_{X_1^c}) - V_{s^a p^c}^2 \frac{E_{s*a} - E_{X_1^c}}{E_{s^a} - E_{X_1^c}} \right]^{1/2} \ . \tag{A24}$$

Here, $E_{X_1^c}$, $E_{\Gamma_1^c}$, and so on the symmetry point energies of the reference band, and E_{s^a}, E_{s*c}, and so on are the atomic level energies. Vogl's universal model[9] was used to derive the formula given above. The following condition is assumed:

$$U_{pp\pi}^a + U_{pp\pi}^c = 0 \ , \tag{A25}$$

in order to conserve the trace of the Hamiltonian over

the entire Brillouin zone which is conserved when the first-nearest-neighbor interactions alone are included.

APPENDIX B: CALCULATION OF THE OPTICAL MATRIX ELEMENTS

The optical matrix elements $\langle \Gamma_c | M | \Gamma_v \rangle$ appearing in Eq. (3.1) can be evaluated in terms of the function

presented in Eq. (A1):

$$\langle \Gamma_c \mid M \mid \Gamma_v \rangle = \sum_{\substack{m,m' \in A,B \\ b,b'=a,c,a'c' \\ \beta,\beta'=s,p_x,\cdots}} f_\beta^b(m;\Gamma_c) f_{\beta'}^{b'}(m';\Gamma_v)$$

$$\times \langle \phi_\beta^b(m) \mid M \mid \phi_{\beta'}^{b'}(m') \rangle ,$$

(B1)

with

$$\langle \Gamma_c \mid M \mid \Gamma_v \rangle = e^{i\mathbf{K}\cdot\mathbf{r}} \langle \Gamma_c \mid p \mid \Gamma_v \rangle ,$$

where $f_\beta^b(m;\Gamma_c)$ stands for the expansion coefficients in Eq. (A1) for the Γ point of the lowest conduction band, and the suffixes β and β' indicate the atomic orbital (i.e., s, p_x, p_y, p_z, or s^*) which is not explicitly written in Eq. (A1). $\mid \phi_\beta^b(m) \rangle$ shows the β-orbital function of the atoms in the mth sublayer in A or B material. The evaluation of the momentum matrix elements $\langle \Gamma_c \mid p \mid \Gamma_v \rangle$ in the empirical sp^3s^* tight-binding scheme has been done by Schulman and Chang[24] for GaAs/Al$_x$Ga$_{1-x}$As superlattices. In their work, the momentum matrix elements were evaluated from the results of a full-zone $\mathbf{k}\cdot\mathbf{p}$ calculation. In the present work, however, the numerical atomic orbitals attained by the Herman-Skillman-type[18] program are employed and the momentum matrix elements between $s(s^*)$ and p states are computed directly. The momentum matrix elements between atomic orbitals at different sites are neglected for the sake of simplicity, since the order of magnitude of the estimated oscillator strength may not be affected much of this simplification. As for this simplification, similar treatment has been done by Drummond *et al.*[25]

APPENDIX C: PRESSURE DEPENDENCE OF TIGHT-BINDING PARAMETERS

The effect of applying pressure to the superlattice is taken into account by renormalizing the tight-binding parameters. The pressure dependence of the tight-binding parameters is derived from the change of interatomic distance through the d^{-2}-scaling rule.[19] The change of interatomic distance can be estimated from the elastic moduli when a stress tensor is given. In the case of a cubic system, the relation between stress and strain tensors is given by

$$\begin{bmatrix} T_{11} \\ T_{22} \\ T_{33} \\ 2T_{23} \\ 2T_{31} \\ 2T_{12} \end{bmatrix} = \begin{bmatrix} c_{11} & c_{12} & c_{12} & 0 & 0 & 0 \\ c_{12} & c_{11} & c_{12} & 0 & 0 & 0 \\ c_{12} & c_{12} & c_{11} & 0 & 0 & 0 \\ 0 & 0 & 0 & c_{44} & 0 & 0 \\ 0 & 0 & 0 & 0 & c_{44} & 0 \\ 0 & 0 & 0 & 0 & 0 & c_{44} \end{bmatrix} \begin{bmatrix} e_{11} \\ e_{22} \\ e_{33} \\ e_{23} \\ e_{31} \\ e_{12} \end{bmatrix}$$

(C1)

where c_{11}, c_{12}, and c_{44} are elastic moduli; e_{11}, e_{22}, e_{33}, e_{23}, e_{31}, and e_{12} are components of the strain tensor; and

T_{11}, T_{22}, T_{33}, T_{23}, T_{31}, and T_{12} are components of the stress tensor. Suffixes 1, 2, and 3 stand for x, y, and z directions, respectively.

1. Hydrostatic pressure

The application of hydrostatic pressure is represented by the following stress tensor:

$$T_{11} = T_{22} = T_{33} \neq 0 ,$$
$$T_{23} = T_{31} = T_{12} = 0 .$$

(C2)

In this case, the following components of the strain tensor are derived from Eq. (C1) as

$$e_{11} = e_{22} = e_{33} = \frac{T_{11}}{c_{11} + 2c_{12}} ,$$

(C3)

where T_{11} is the magnitude of the applied hydrostatic pressure. The bond length l under hydrostatic pressure is given by

$$l = (1 - e_{11})l_0 ,$$

(C4)

where l_0 denotes the bond length in the original material without pressure. Then the tight-binding parameters of the first- and second-nearest-neighbor interactions can be renormalized as

$$V = (1 - e_{11})^{-2}V_0 ,$$
$$U_{pp\pi}^{b(b')} = (1 - e_{11})^{-2}U_{pp\pi 0}^{b(b')} ,$$
$$U_{pp\pi}^{bb(bb')} = (1 - e_{11})^{-2}U_{pp\pi 0}^{bb(bb')} .$$

(C5)

Here, the elements V, $U_{pp\pi}^{b(b')}$, and $U_{pp\pi}^{bb(bb')}$ are a first- and two second-nearest-neighbor parameters defined in Appendix A. The subscript 0 indicates the quantity under no pressure.

2. Parallel uniaxial pressure

When uniaxial pressure is applied parallel ($\parallel$, "1" direction) to the superlattice layer, the applied stress is represented by

$$T_{11} \neq 0 ,$$
$$T_{22} = T_{33} = 0 ,$$
$$T_{23} = T_{31} = T_{12} = 0 .$$

(C6)

The induced components of the strain tensor are calculated as

$$e_{11} = \frac{c_{11} + c_{12}}{(c_{11} - c_{12})(c_{11} + 2c_{12})}T_{11} ,$$
$$e_{22} = e_{33} = \frac{-c_{12}}{(c_{11} - c_{12})(c_{11} + 2c_{12})}T_{11} ,$$

(C7)

and the pressure dependence of the tight-binding parameters is given by the formulas

$$V = V_0 \frac{3}{(1-e_{11})^2 + 2(1-e_{12})^2} \ ;$$

$$U_{pp\pi}^{b(b')} = U_{pp\pi0}^{b(b')} \frac{2}{(1-e_{11})^2 + (1-e_{12})^2} \ ;$$

$$^{(x)}U_{pp\pi}^{bb(bb')} = U_{pp\pi0}^{bb(bb')} \frac{2}{(1-e_{11})^2 + (1-_{12})^2} \ ; \tag{C8}$$

$$^{(y)}U_{pp\pi}^{bb(bb')} = U_{pp\pi0}^{bb(bb')} \frac{1}{(1-e_{12})^2} \ .$$

Here, $^{(x)}U_{pp\pi}^{bb(bb')}$ and $^{(y)}U_{pp\pi}^{bb(bb')}$ represent the second-nearest-neighbor interactions between two atoms having the same x and y coordinates, respectively.

3. Perpendicular uniaxial pressure

When uniaxial pressure is applied perpendicular ($\perp$, "z" direction) to the superlattice layer, the applied stress can be represented by

$$T_{11} = T_{22} = 0 \ ,$$

$$T_{33} \neq 0 \ , \tag{C9}$$

$$T_{23} = T_{31} = T_{12} = 0 \ .$$

The induced components of the strain tensor are then calculated as

$$e_{11} = e_{22} = \frac{-c_{12}}{(c_{11}-c_{12})(c_{11}+2c_{12})} T_{33} \ ,$$

$$e_{33} = \frac{c_{11}+c_{12}}{(c_{11}-c_{12})(c_{11}+2c_{12})} T_{33} \ , \tag{C10}$$

and the pressure dependence of the tight-binding parameters is given by the formulas

$$V = V_0 \frac{3}{(1-e_{11})^2 + 2(1-e_{12})^2} \ .$$

$$U_{pp\pi}^{b(b')} = U_{pp\pi0}^{b(b')} \frac{1}{(1-e_{12})^2} \ , \tag{C11}$$

$$U_{pp\pi}^{bb(bb')} = U_{pp\pi0}^{bb(bb')} \frac{2}{(1-e_{11})^2 + (1-e_{12})^2} \ .$$

[1]E. Finkman, M. D. Sturge, and M. C. Tamargo, Appl. Phys. Lett. **49**, 1299 (1986).

[2]N. Hamada and S. Ohnishi, Phys. Rev. B **34**, 9042 (1986).

[3]T. Nakayama and H. Kamimura, J. Phys. Soc. Jpn. **54**, 4726 (1985).

[4]M. A. Gell, D. Ninno, M. Jaros, D. J. Wolford, T. F. Keuch, and J. A. Bradley, Phys. Rev. B **35**, 1196 (1987).

[5]J. Ihm, Appl. Phys. Lett. **50**, 1068 (1987).

[6]U. Gnutzmann and K. Clausecker, Appl. Phys. **3**, 9 (1974).

[7]J. Y. Kim and A. Madhukar, J. Vac. Sci. Technol. **21**, 528 (1982).

[8]J. N. Schulman and T. C. McGill, Phys. Rev. B **19**, 6341 (1979).

[9]M. Kumagai, T. Takagahara, and E. Hanamura, Solid State Commun. **64**, 659 (1987).

[10]P. Vogl, H. P. Hjalmarson, and J. D. Dow, J. Phys. Chem. Solids **44**, 365 (1983).

[11]K. E. Newman and J. Dow, Phys. Rev. B **30**, 1929 (1984).

[12]E. Yamaguchi, Jpn. J. Appl. Phys. **25**, L643 (1986).

[13]J. R. Chelikowsky and M. L. Cohen, Phys. Rev. B **14**, 556 (1976).

[14]Y. F. Tsay, A. J. Corey, and S. S. Mitra, Phys. Rev. B **12**, 1354 (1975).

[15]D. J. Chadi and M. L. Cohen, Phys. Status Solidi B **68**, 405

(1975).

[16]J. Tersoff, J. Vac. Sci. Technol. B **4**, 1066 (1986).

[17]R. S. Knox, *Theory of Excitons* (Academic, New York, 1963), Suppl. 5.

[18]F. Herman and S. Skillman, *Atomic Structure Calculations* (Prentice-Hall, New Jersey, 1963).

[19]W. A. Harrison, *Electronic Structure and the Properties of Solids* (Freeman, San Francisco, 1980).

[20]*Physics of Group IV Elements and III-V Compounds*, Vol. 17a of *Landolt-Börnstein*, edited by O. Madelung, M. Schultz, and H. Weiss (Springer, Berlin, 1982).

[21]W. F. Boyle and R. J. Sladek, Phys. Rev. B **11**, 2933 (1975).

[22]T. P. Pearsall, J. Bevk, L. C. Feldman, J. M. Bonar, J. P. Mannarets, and A. Ourmazd, Phys. Rev. Lett. **58**, 729 (1987).

[23]J. Bevk, A. Ourmazd, L. C. Feldman, T. P. Pearsall, J. M. Bonar, B. A. Davidson, and J. P. Mannaerts, Appl. Phys. Lett. **50**, 760 (1987).

[24]J. N. Schulman and Yia-Chung Chang, Phys. Rev. B **31**, 2069 (1985).

[25]T. J. Drummond, E. D. Jones, H. P. Hjalmarson, and B. L. Doyle, in *Proceedings of the 13th International Symposium on Gallium Arsenide and Related Compounds*, edited by W. T. Lindley (IOP, Brisol, 1986), p. 331.